Analysis of Multi-Band Circle MIMO Antenna Design for C-Band Applications

Kommana Vasu Babu[1], [*] and Bhuma Anuradha[2]

Abstract—In this paper a novel design to reduce mutual coupling in circular patch antennas is proposed. A circular MIMO antenna with a dumb-bell shape parasitic element is inserted between the two circular patch antennas thereby reducing the mutual coupling. It has been observed that the proposed design produces multi-band characteristics at 3.1 GHz, 6.2 GHz & 7.7 GHz. At the tri-band frequencies impedance bandwidths (IBW's) are around 90 MHz, 320 MHz, and 540 MHz. The process involves cutting rectangular slits on each side of a circular patch and placing a dumb-bell shaped parasitic structure to reduce the transmission coefficient (S_{12}) to -40.75 dB. It is observed that the antenna parameters are greatly improved in terms of ECC, diversity gain, directivity, group delay, and peak gain which are are 0.005, 9.973 dBi, 6.14 dBi, 10.81 ± 1 nsec, and 3.59 dBi. The results of experimental validation and numerical analysis are presented. The antenna design can be used for wireless communication as well as all C-band applications.

1. INTRODUCTION

In wireless communication technology, a number of new developments have led to improved wideband characteristics, improvement in isolation, good polarization diversity, orthogonality performance, and design of simple structures. These structures support WiMAX (5.48–5.74 GHz), UWB ranges (3.1–10.3 GHz), ITS (5.84–5.92 GHz) for single platform vehicular communication, and WLAN (5.14–5.34 GHz & 5.72–5.82 GHz). Various dual/tri-feed/quad feed/multi and single band antennas have been observed [1–25]. Planar UWB easily extendable array antenna is operated at a frequency 3.1–16.0 GHz producing a gain of 4 dBi, and ECC is 0.025 with an occupied area of $38 \times 90 \, \text{mm}^2$ [1]. By using split-ring resonator (SRR) polarized MIMO analysis shows a low ECC around 0.001 while with a compact antenna area $40.5 \, \text{mm} \times 40.5 \, \text{mm}$ [2], S_{12} is greater than -20 dB. In [3], a slot antenna for diversity applications has produced S_{12} of -21 dB operating between 2.8 and 11.0 GHz. Minkowski MIMO has multi-band frequencies [4] reducing isolation greatly to -52 dB with cutting rectangular slots on an around patch MINI antenna. A novel printed filtenna with a dimension of $35 \times 68 \, \text{mm}^2$ produced a dual-band of frequencies which maintain an isolation ≤ -20 dB with a peak gain ≥ 3.5 dBi in [5] and identify better out-band characteristics at the resonant frequencies. For mobile terminal applications, using a G-shaped slot [6] on the radiator results in a peak gain 4.78 dBi, ECC maintained less than 0.04, and occupied area $4100 \, \text{mm}^2$. In [7], star, H, circular, I, and square shape EBG structures were identified which increased the gain, improved S_{11}, reduced isolation with compact dimensions of $35 \, \text{mm} \times 40 \, \text{mm}$. A compact stepped slot UWB design of $44 \times 44 \, \text{mm}^2$ had an ECC 0.04, peak gain 3.8 dBi, and a mutual coupling value less than -15 dB [8] by suppression of common-mode. In [9], a UWB MIMO design had a size of $60 \times 48 \, \text{mm}^2$ and produced dual-band antenna with a band-notched function. An inverted F-shape antenna, square ring dual-polarized for radar, UWB & imaging applications has

* Corresponding author: Kommana Vasu Babu (vasubabuece@gmail.com).
[1] Department of Electronics & Communication Engineering, Vasireddy Venkatadri Institute of Technology, Nambur, Guntur, A.P, India. [2] Department of Electronics & Communication Engineering, Sri Venkateswara University, Tirupathi, A.P, India.

been proposed, and using black film carbon technology [10–12] has resulted in suppressing the mutual coupling. To enhance wider-band isolation [13], a tree structure with small size of $35 \times 40 \, \text{mm}^2$ covering 3.1–10.6 GHz has $S_{12} < -20$ dB. A Dual Band Notched [14] MIMO diversity radiator for UWB wireless system applications maintained an ECC value ≤ 0.08 was observed. A loop antenna had a meandered structure using [15, 16] WLAN and LTE operated 1760–2630 MHz & 675–1098 MHz and integrated DGS for patch antenna. A packed antennas having $20 \times 40 \times 1.6 \, \text{mm}^3$ with center-to-center distance $0.05\lambda_0$ was designed to enhance isolation [17]. A tri-band notched MIMO had a transmission coefficient -39 dB and reflection coefficient -41 dB and an overall occupied area of $3136 \, \text{mm}^2$ [18]. A dual inverted F-shaped dual-band antenna had a size of $74 \, \text{mm} \times 150 \, \text{mm}$, decoupled building block [19] of eight antennas of dual-band 3.5/5.8-GHz MIMO radiator for smart phone application. A compact co-planar waveguide (CPW) fed hexagonal ring antenna having monopole elements [20] with ground plane was connected operating from 3.0 to 12.0 GHz with ECC ≤ 0.18 and $S_{12} \leq -15$ dB. In [21], a $27.2 \times 46 \, \text{mm}^2$ UWB MIMO antenna exhibits a number of stopbands using a compact radiator; efficiency varies from 78 to 96.7%; peak gain varies from 1.4 dBi to 4 dBi; ECC is 0.018; DG was approximately 10 dB. A CSRR UWB diversity antenna [22] operating from 3 to 12 GHz has an efficiency of 82%, and gain value is 4.7 dBi, and ECC < 0.15 with a compact size $23 \, \text{mm} \times 29 \, \text{mm}$. In [23], it is observed that the performance evaluation of 5G communication having dual-mode & triple-band MIMO 10-antenna handset array antenna maintains ECC ≤ 0.05. A triband MIMO antenna [24] has a size of $40 \times 35 \, \text{mm}^2$ for WiMAX, radio astronomy and WLAN applications with reduced isolation (S_{12}) around -52 dB. In [25], a compact multi-band MIMO radiator improved the isolation parameter greatly. In this research paper, an interesting observation has been made that a radiator having a total area of $40 \, \text{mm} \times 40 \, \text{mm}^2$ was greatly improved with S_{11} of -46.8 dB, S_{12} of -40.75 dB, operating range of frequencies from 2.0 to 10.0 GHz, a peak gain of 4.16 dBi, and ECC as low as 0.005. Table 1 shows the parameters of the proposed radiator compared with the previously existed systems.

Table 1. Comparison with other existing works.

Parameters	[5]	[9]	[14]	[19]	[23]	This work
Dimensions (mm²)	35×68	60×48	26×28	40×70	35×50	40×40
	-25	-28	-32	-27	-36	-18
S_{11} (dB)	-29	-32	-26	-33	-28	-48.2
						-41.2
	-28	-17.2	-25	-38	-34	-35
S_{12} (dB)	-31	-28	-32	-23.5	-37	-40.75
						-42
	3.3–3.5	3.4–3.7	5.0–5.8	3.4–3.6	3.4–3.8	3.10–3.19
Bandwidth (GHz)	5.6–5.9	5.15–5.85	6.6–7.4	5.7–5.8	5.1–5.9	6.11–6.43
						7.50–8.04
	3.8	4.6	4.18	3.2	5.8	4.52
Peak gain (dBi)	4.2	2.8	3.54	4.7	3.9	6.47
						5.86
	0.002	0.0018	0.08	0.05	0.03	0.005
ECC	0.006	0.0027	0.06	0.03	0.45	0.007
						0.002

2. ANTENNA DESIGN

The geometry of circular MIMO parasitic element antenna design and its fabricated structure are shown in Fig. 1. This antenna is fabricated on an FR-4 substrate, with loss tangent 0.02 and relative permittivity 4.4. The antenna comprises an FR4 substrate, ground plane, and two circular patches. A circular patch is placed on the left as well as the right side with a separation of $0.25\lambda_0$. In this circle
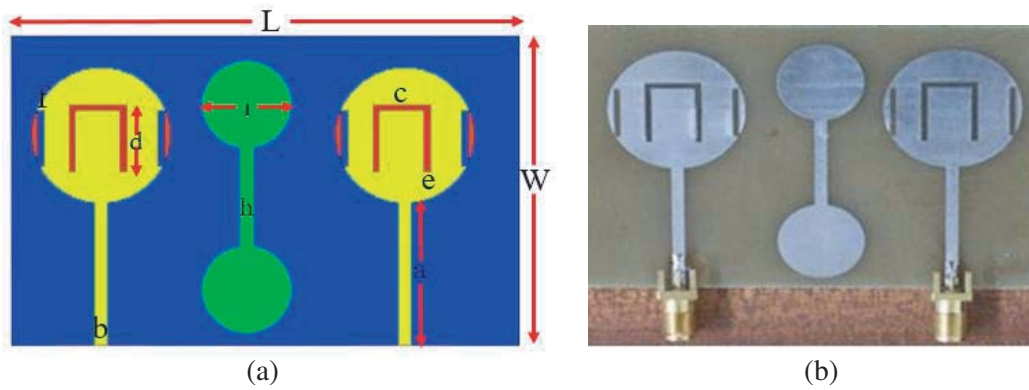
Figure 1. Circle MIMO antenna design representation. (a) Circle MIMO antenna design. (b) Fabricated design.

Table 2. Circle MIMO antenna design with parasitic structure dimensions.

Design parameter	L	W	a	b	c	d	e	f	g	h	i	ε_r
Value (mm)	40	40	24	2	3	5	2	2	10	3	10	4.4

MIMO approach DMS in circular patches and inserting a dumbbell-shaped slot between the patches reduces the mutual coupling greatly. This approach results in three resonating bands 3.10–3.19 GHz (Wireless communication), 6.11–6.43 GHz & 7.50–8.04 GHz (C-band applications). The antenna has a compact size of 40 mm × 40 mm with 1.6 mm as the thickness of substrate. FIT based technique is used for investigation of parametric study of the proposed system, and a 50 Ω MS line is used for excitation. The optimized dimensions of proposed system are listed in Table 2. By choosing proper dimensions of MIMO antenna design, the EM interaction between the patches is reduced to required level, thereby improving the performance parameters.

Different stages of the evaluation of the proposed structure are shown in Fig. 2. Antenna #1

Antenna #1

Antenna #2
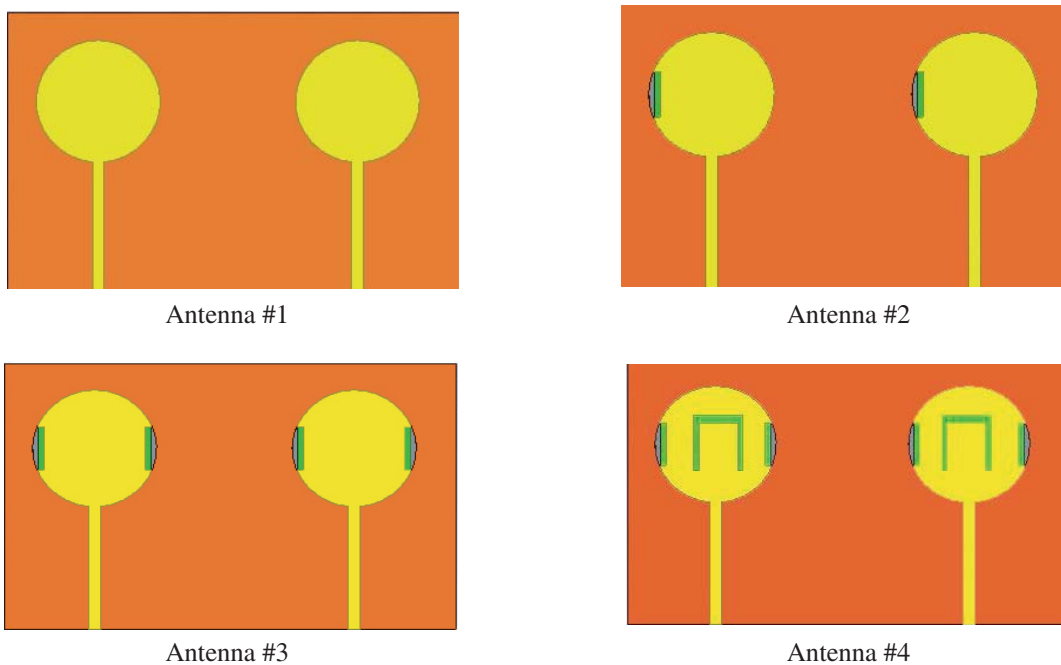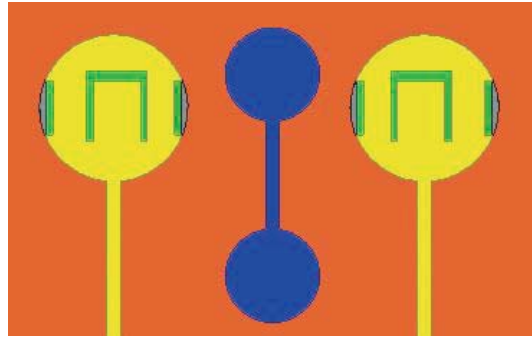
Antenna #3

Antenna #4

Antenna #5

Figure 2. Circle MIMO antenna design evaluation stages.
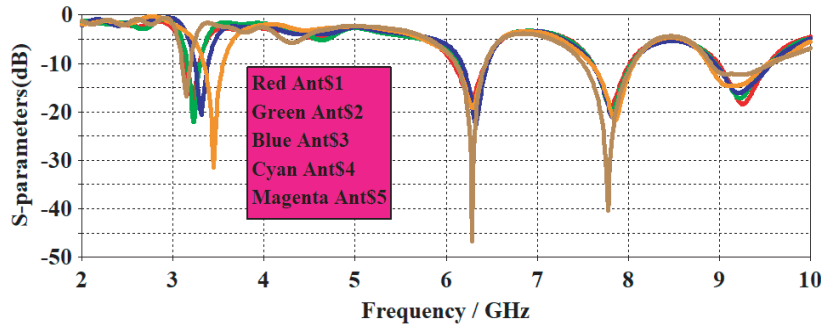
Figure 3. S_{11} of step by step antenna process.
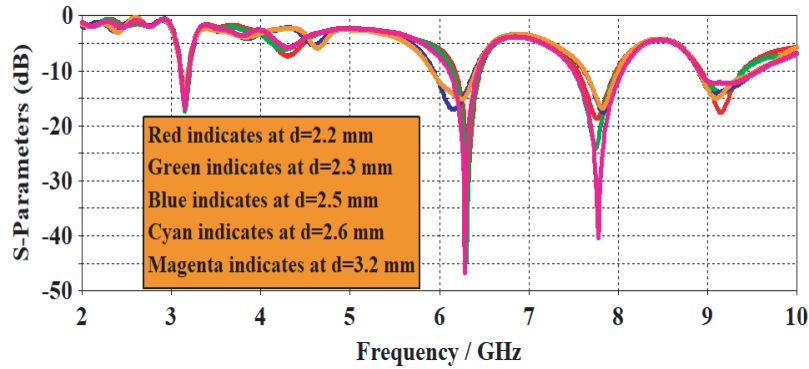
Figure 4. S_{11} parametric analysis for different distance variations.

indicates the patch antenna having two circular patches arranged in a rectangular patch to produce three bands whose $S_{11} < -20$ dB. Antenna #2 is designed with small rectangular slots cut on left and right sides of circular patch, and produces three bands whose $S_{11} < -22$ dB. Antenna #3 represents the left and right side rectangular slots on the circular patch and produces three bands whose $S_{11} < -21$ dB. Antenna #4 indicates that an inverted U-shaped slot is inserted on the middle of circular patch whose $S_{11} < -16$ dB. Finally, Antenna #5 represents a dumb-bell shaped slot inserted between the two circular patches to produce three bands with $S_{11} < -30$ dB. For each stage the reflection coefficient is shown in Fig. 3. By varying this step by step procedure, the reflection coefficient varies less than -10 dB for all the cases. Fig. 4 & Fig. 5 shows that the the distance is varied between the two patches $d = 2.2$ mm, $d = 2.3$ mm, $d = 2.5$ mm, $d = 2.6$ mm, and $d = 3.2$ mm in parametric analysis of proposed design and
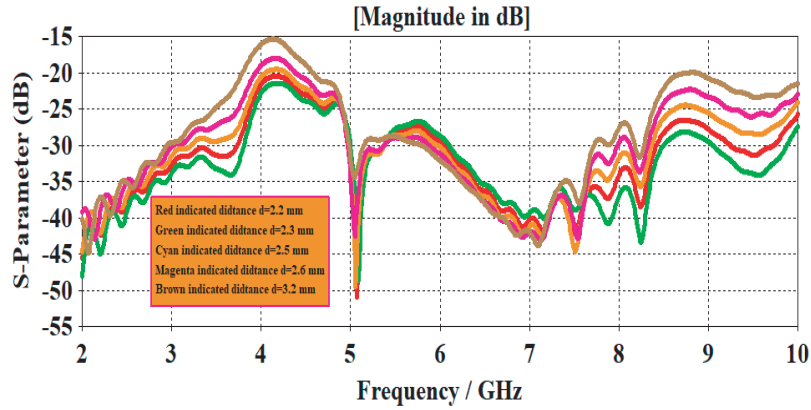
Figure 5. S_{12} parametric analysis for different distance variations.

observes that there is a little bit variations in S_{11} and changes in S_{12} for different mentioned distances varied at the three resonate bands of frequencies -30 dB to -60 dB. A particular separation distance of $d = 2$ mm between the radiating patches produced around -48 dB greatly minimizes the EM interaction between the patches. In this case, the antenna radiates efficiently, and investigation of analysis pattern at different frequency components minimizes the mutual coupling when the two antennas are close to each other.

3. THEORETICAL ANALYSIS

The width (W) of MSPA is evaluated from

$$W = \frac{c}{2f_r\sqrt{\dfrac{\varepsilon_r + 1}{2}}} \tag{1}$$

where

$f_r =$ resonant frequency
$c =$ Velocity of light
$\varepsilon_r =$ Substrate dielectric constant
The length (L) of MSPA is evaluated from

$$L = \frac{\lambda_0}{2f_r\sqrt{\varepsilon_{reff}}} - 2\Delta L \tag{2}$$

where

$\varepsilon_{eff} =$ substrate effective dielectric constant
$\lambda_0 =$ free space wavelength
$\Delta L =$ increase in length.

$$\Delta L = 0.412h\left[\frac{(\varepsilon_{reff} + 0.3)\left(\dfrac{W}{h} + 0.264\right)}{(\varepsilon_{reff} - 0.258)\left(\dfrac{W}{h} + 0.8\right)}\right] \tag{3}$$

Here

$h =$ substrate height
$\varepsilon_{eff} =$ effective dielectric constant

$$\varepsilon_{reff} = \frac{\varepsilon_r + 1}{2} + \frac{\varepsilon_r - 1}{2} \left[1 + 12\frac{h}{W} \right]^{-\frac{1}{2}} \tag{4}$$

Effective length of the antenna is given by

$$L = L_{eff} + 2\Delta L \tag{5}$$

4. RESULT ANALYSIS DISCUSSION

The simulated and experimentally verified results are as shown in Fig. 6. The simulated isolation is greater than $-10\,\mathrm{dB}$ for the entire operating band. Our proposed design has a tri-band antenna: 3.10–3.19, 6.11–6.43 & 7.50–8.04 GHz covering the wireless communication and C-band applications. The observations in Fig. 7 reveal a slight variation in the three resonating bands of frequencies between measured and experimental VSWRs. The first frequency resonates at 3.1 GHz. It is observed that the measured band is also resonant at the same frequency, but the value decreases at approximately $-12.45\,\mathrm{dB}$. The second band resonates at 6.2 GHz, and it is observed that the measured frequency slightly shifted to left side of simulated frequency, a little bit variations at 6.1 GHz. This happens because variation in S_{11} of $-25\,\mathrm{dB}$ is observed in alignment measurement in soldering of SMA connector. The final resonant band is at 7.7 GHz, and it is observed that the measured result has a small variation at the frequency 7.8 GHz with a S_{11} of $-22\,\mathrm{dB}$. Another important parameter in the design of MIMO antenna
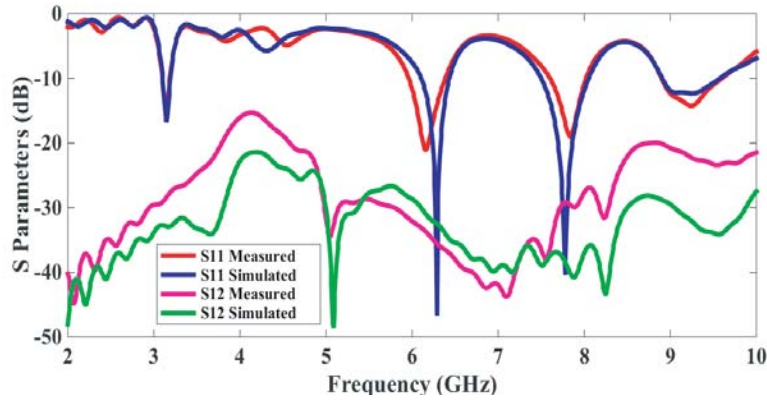
Figure 6. S-parameters comparison practical & simulation.
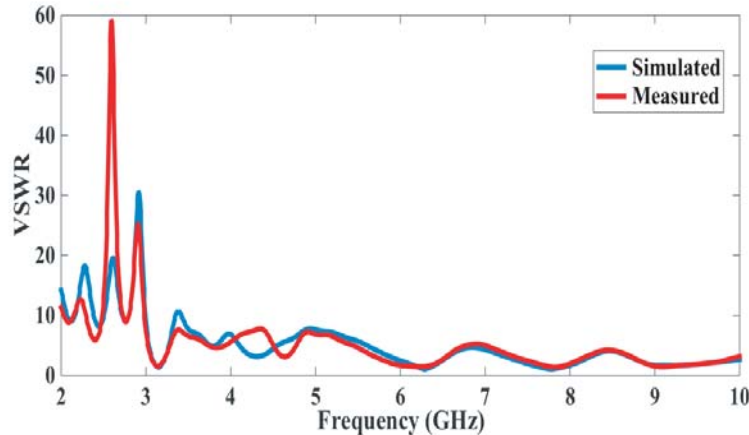
Figure 7. Analysis of VSWR.

analysis is its transmission coefficient (S_{12}) as observed in the parametric approach by placing different distances between the patches to maintain low EM interaction. By checking on the various distances between the patches it is concluded that at one particular distance the parameter mutual coupling is greatly reduced, and this distance is fixed to measure S_{12} in the parametric study analysis. At that particular distance it is observed that S_{12} is ≤ -15 dB. For the first resonating band of frequency, the simulated value is -35 dB, and measured value is -28 dB, in which a slight variation is observed. At the second resonant frequency it is observed that the simulated value is -39 dB, and measured value is -33 dB. Finally at the third resonant band of frequency, it is observed that the simulated value is
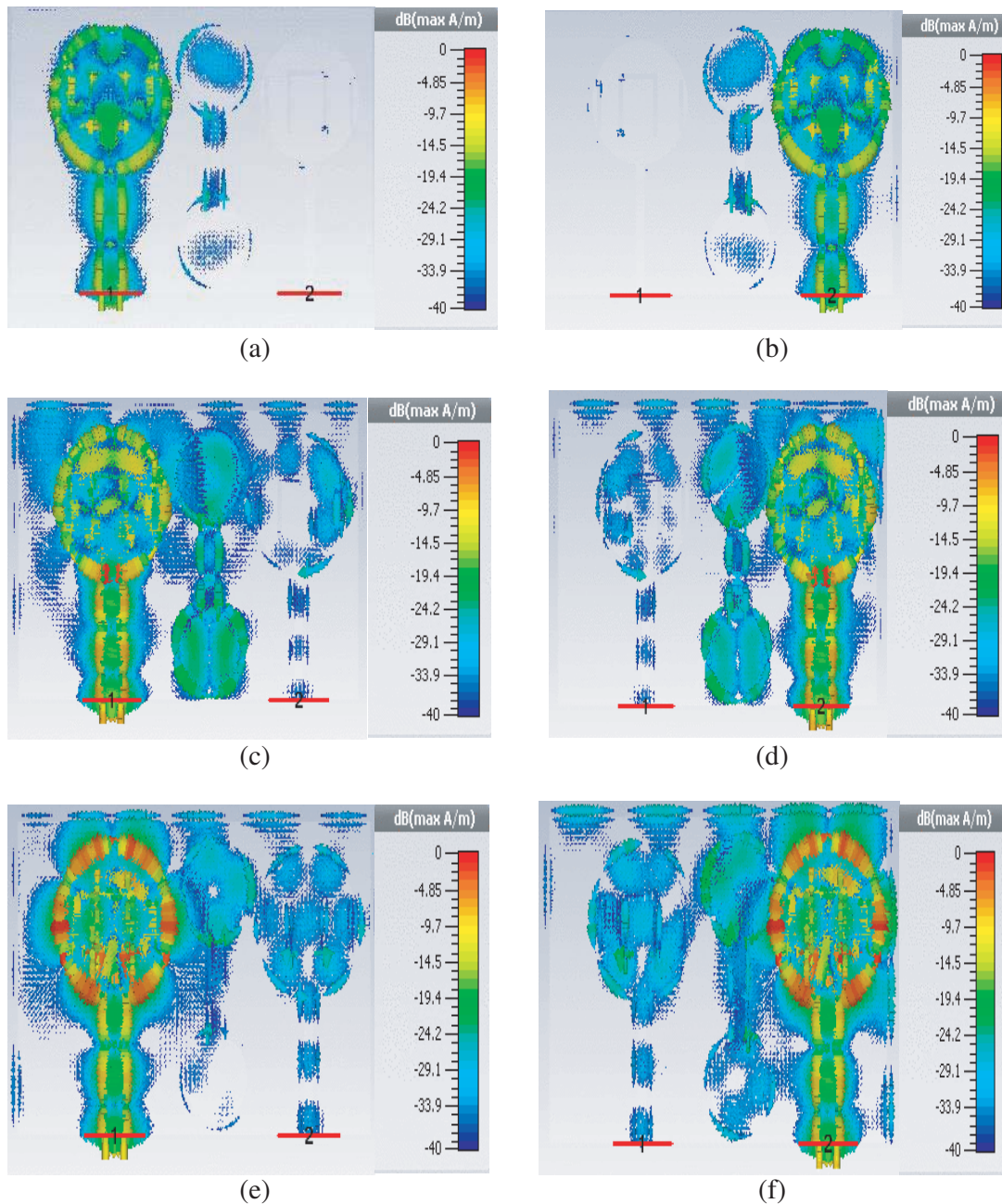
Figure 8. Frequencies at 3.1 GHz, 6.4 GHz & 7.8 GHz surface current distribution. (a) Port #1 is excited, (b) Port #2 is excited, (c) Port #1 is excited, (d) Port #2 is excited, (e) Port #1 is excited, (f) Port #2 is excited.

−42 dB, and measured value is −34 dB. At three resonating bands of frequencies, the proposed circle MIMO dumbbell-shaped parasitic element greatly improves the reduction of mutual coupling compared to the other existing approaches mentioned earlier. From the VSWR comparison it is observed that a slight variation is noticed between practical and simulated VSWRs, which is less than or equal to 2 at three resonant band of frequencies as shown in Fig. 7.

The distributions of surface current nature at three resonant frequencies are identified in Figs. 8(a)–(f), respectively, with port #2 terminated with 50 ohms load and exciting port #1. From Fig. 8(a), it can be clearly observed how the surface wave propagates from antenna 1 to antenna 2 and that more current passes at the center of circular patch and minimum current in the parasitic structure. Here the introduction of a parasitic structure between the patches has reduced the density of current in antenna 2 compared to the MIMO antenna in the case without parasitic structure. In Fig. 8(b) it is observed that port #2 is excited and port #1 terminated with 50 ohm load. The distribution of electric filed inside the MIMO substrate is significantly reduced with parasitic structure, and the isolation behavior
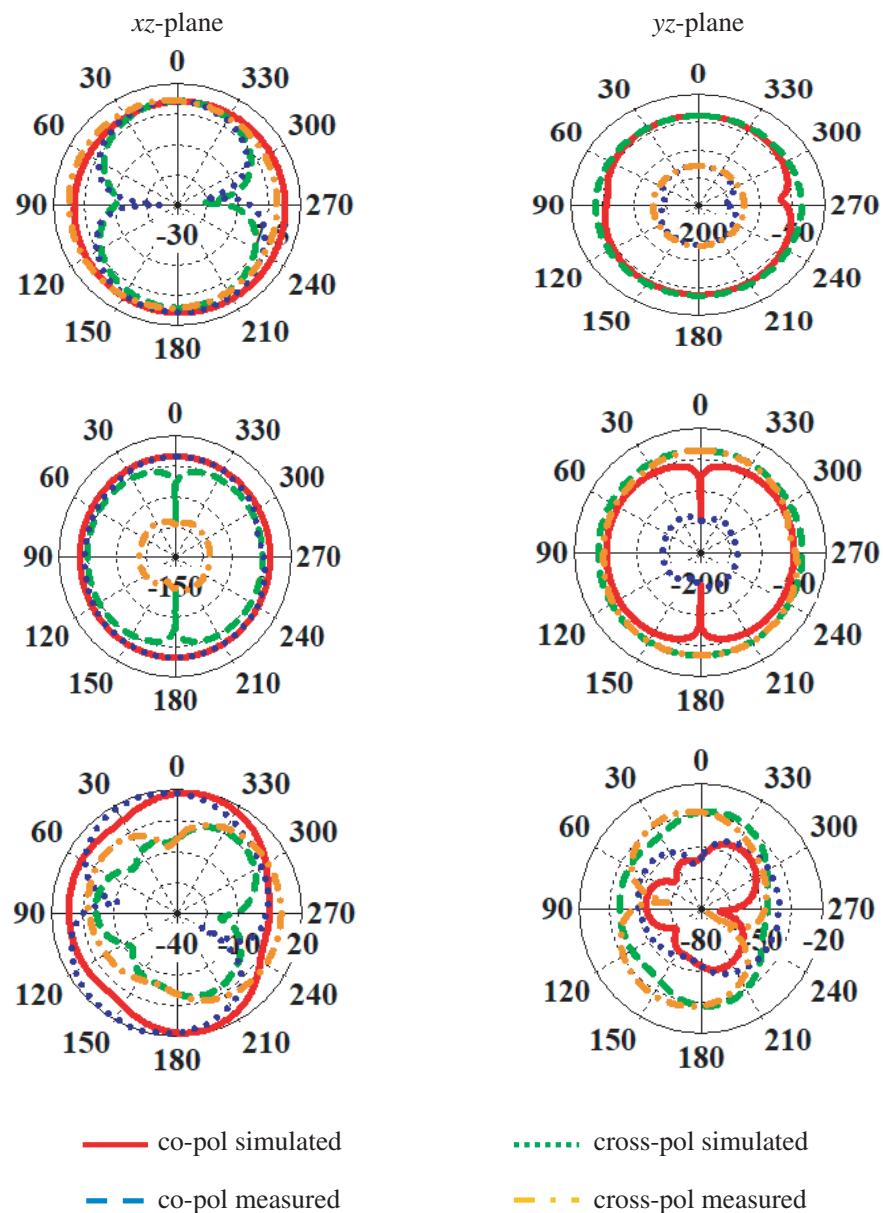
Figure 9. Frequencies at 3.1, 6.4 & 7.8 GHz radiation patterns representation.

strengthens the parasitic structure by restricting the propagation of space wave from Antenna #1 to Antenna #2 and vice-versa. From Fig. 8(c) it can be observed that Antenna #1 is excited and Antenna #2 terminated with 50 ohm load. In this case, it is observed that there is a lot of variations in the distribution of current, and a parasitic structure in between the patches produces maximum current. Similarly from Figs. 8(d)–(f) it is observed that the distribution currents circulate inside the circular patches, and maximum current will flow inside the entire patch.

The three resonating bands have been indicated. Antenna 1 is excited and antenna 2 terminated, and vice versa. xz plane (E-plane) and yz-plane (H-plane) patterns of normalized radiations are shown in Fig. 9. The purpose of MIMO antenna is to achieve almost omnidirectional radiation pattern, and thus the signal is attained irrespective of the direction arrival with the help of its corresponding radiating antenna elements. It is observed that the xz-plane (E-plane) in Fig. 9 is preserved resulting in omnidirectional radiation pattern at three resonating frequencies. Co- and-cross polarizations show their behaviors of isolation in xz-plane (E-plane) except for limited points.

In Fig. 10 the real part of impedance S_{11} of circle MIMO parasitic element can be observed, and the imaginary part is also represented in Fig. 10. The real part of this design S_{11} of input impedance shows that the resonant peaks are at 3.1 GHz, 6.2 GHz, and 7.7 GHz in the frequency range from 2.0–10.0 GHz represent a parallel circuit of RLC components connected in series. The simulated imaginary part impedance graph shows that it is inductive in nature, and more resistance value is around 50, showing a parallel behavior of RLC circuit in parallel. From Fig. 10 it is observed that a sharp peak of resistance observed at 6.2 GHz represents RLC circuit in parallel. The resonant band of circuit shows that two RLC parallel circuits are connected in series. Fig. 11 indicates the representation of group delay measured by keeping two identical antennas excited in the far-field distance which corresponds to the lowest frequency in the operating band side with side and face to face orientation. In both the cases it is observed that port #1 is excited and port #2 terminated with 50 ohms load, and vice versa.
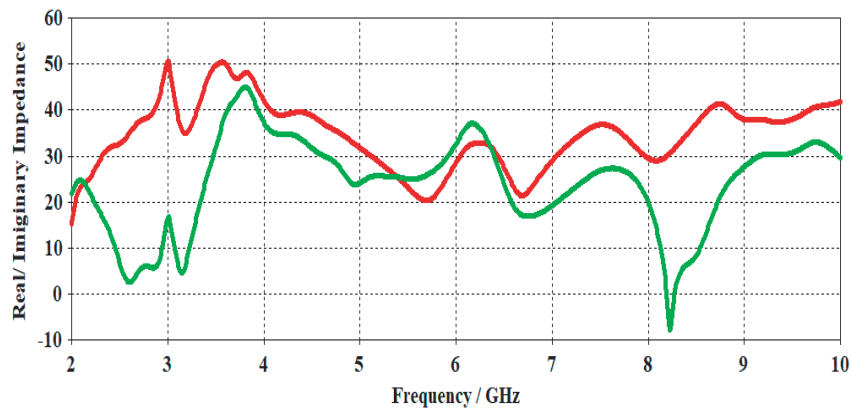
Figure 10. Circle MIMO antenna impedance (Real & Imaginary) analysis.
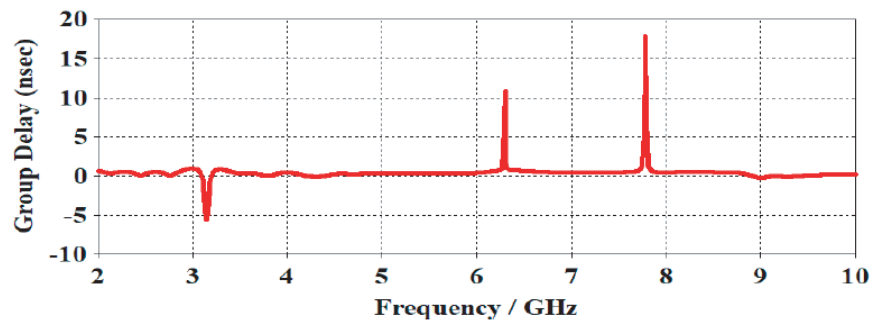
Figure 11. Circle MIMO antenna group delay analysis.
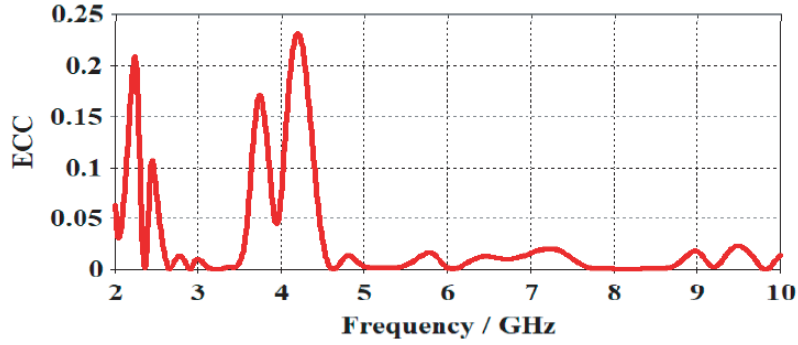
Figure 12. Circle MIMO ECC analysis.

From Fig. 11, it is observed that group delay is constant throughout the operating band except at three resonating frequencies which are $3.1\,\text{GHz}$, $6.2\,\text{GHz}$ & $7.7\,\text{GHz}$. The group delay values at three resonant frequencies are observed as $-5.3\,\text{nsec}$, $12\,\text{nsec}$ and $18\,\text{nsec}$.

For any MIMO antenna, the performance of diversity is calculated using envelope correlation coefficient (ECC), diversity gain (DG), and figures-of-merit. For the isolated and correlated communication channels, the total occupied distribution volume is evaluated using ECC. For practical limitation uncorrelated antenna diversity is ECC < 0.5, but ideally its value is zero. From S-parameters the ECC for the first and second antennas is evaluated using Equation (6). The ECC of MIMO parasitic element is shown in Fig. 12, and this value becomes zero which represents good diversity. When the value of ECC reaches 0.24 at the lower resonating band, there is a decrease in the higher resonating band which is observed in MIMO antenna with parasitic design.

$$\text{ECC}(\rho_C) = \left| \frac{\displaystyle\iint_{4\pi} |S_{11}^* S_{21} + S_{21}^* S_{22}|}{\left[\left(1 - \left(|S_{11}|^2 + |S_{21}|^2\right)\right) \left(1 - \left(|S_{22}|^2 + |S_{12}|^2\right)\right) \right]^{1/2}} \right| \tag{6}$$

The diversity gain is almost closely related to the envelope correlation coefficient (ECC), and the lower the value of ECC is observed, the higher the value of DG is evaluated using the mathematical relation:

$$\text{DG} = \sqrt{1 - |\rho_c|^2} \tag{7}$$

The DG observed for MIMO parasitic element from Fig. 13 is near the maximum, almost equal to the $10\,\text{dBi}$, which resembles that better diversity performance.
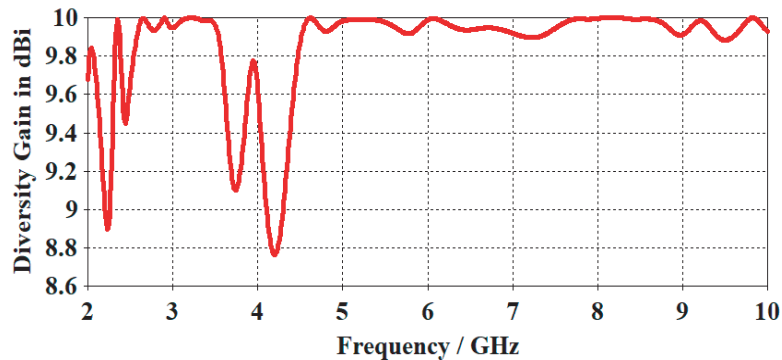
Figure 13. Circle MIMO diversity gain analysis.

5. CONCLUSION

A circular parasitic MIMO antenna with rectangular slits on left and right side of circular patch and inverted U-shaped patch on both circular patches in the three resonating bands of frequencies 3.1, 6.2, 7.7 GHz with a microstrip feeding has been proposed. The process involves cutting rectangular slots, inverted U-shape slots, and dumbbell-shape parasitic element inserted between the patches achieved to suppress the unpreventable mutual coupling. The proposed MIMO antenna has a wider impedance bandwidth with $S_{11} < -10$ dB in three resonating bands of frequencies ranging from 2.0 to 10.0 GHz and has a reduced mutual coupling $|S_{12}| < -25$ dB, which can be deduced from the measured and simulated results. It is interesting to observe that the antenna parameters are greatly improved in terms of ECC, diversity gain, directivity, group delay, and peak gain which are 0.005, 9.973 dBi, 6.14 dBi, 10.81±1 nsec, and 3.59 dBi, respectively.

REFERENCES

1. Sipal, D., M. P. Abegaonkar, and S. K. Koul, "Easily extendable compact planar UWB MIMO antenna array," *IEEE Antennas and Wireless Propagation Letters*, Vol. 16, 2328–2331, 2017.
2. Irene, G. and A. Rajesh, "A dual-polarized UWB-MIMO antenna with IEEE 802.11 ac band-notched characteristics using split-ring resonator," *Journal of Computational Electronics*, 1–9, 2018.
3. Chacko, B. P., G. Augustin, and T. A. Denidni, "Uniplanar slot antenna for ultrawideband polarization-diversity applications," *IEEE Antennas and Wireless Propagation Letters*, Vol. 12, 88–91, 2013.
4. Babu, K. V. and B. Anuradha, "Design of Multi-band Minkowski MIMO Antenna to reduce the mutual coupling," *Journal of King Saud University-Engineering Sciences*, 2018.
5. Li, W. T., et al., "Novel printed filtenna with dual notches and good out-of-band characteristics for UWB-MIMO applications," *IEEE Microwave and Wireless Components Letters*, Vol. 26, No. 10, 765–767, 2016.
6. Toktas, A., "G-shaped band-notched ultra-wideband MIMO antenna system for mobile terminals," *IET Microwaves, Antennas & Propagation*, Vol. 11, No. 5, 718–725, 2016.
7. Elsheakh, D. M. N., M. F. Iskander, E. A. Abdallah, H. A. Elsadek, and H. Elhenawy, "Microstrip array antenna with new 2D-electromagnetic band gap structure shapes to reduce harmonics and mutual coupling," *Progress In Electromagnetics Research C*, Vol. 12, 203–213, 2010.
8. Liu, Y.-Y. and Z.-H. Tu, "Compact differential band-notched stepped-slot UWB-MIMO antenna with common-mode suppression," *IEEE Antennas and Wireless Propagation Letters*, Vol. 16, 593–596, 2017.
9. Tang, T.-C. and K.-H. Lin, "An ultra-wideband MIMO antenna with dual band-notched function," *IEEE Antennas and Wireless Propagation Letters*, Vol. 13, 1076–1079, 2014.
10. Lee, C.-H., S.-Y. Chen, and P. Hsu, "Integrated dual planar inverted-F antenna with enhanced isolation," *IEEE Antennas and Wireless Propagation Letters*, Vol. 8, 963–965, 2009.
11. Krishna, R. V. S. Ram, and R. Kumar, "A dual-polarized square-ring slot antenna for UWB, imaging, and radar applications," *IEEE Antennas and Wireless Propagation Letters*, Vol. 15, 195–198, 2016.
12. Lin, G.-S., et al., "Isolation improvement in UWB MIMO antenna system using carbon black film," *IEEE Antennas and Wireless Propagation Letters*, Vol. 16, 222–225, 2017.
13. Zhang, S., et al., "Ultrawideband MIMO/diversity antennas with a tree-like structure to enhance wideband isolation," *IEEE Antennas and Wireless Propagation Letters*, Vol. 8, 1279–1282, 2009.
14. Zhao, Y., F.-S. Zhang, L.-X. Cao, and D.-H. Li, "A compact dual band-notched MIMO diversity antenna for UWB wireless applications," *Progress In Electromagnetics Research C*, Vol. 89, 161–169, 2019.
15. Chiu, C.-W., C.-H. Chang, and Y.-J. Chi, "A meandered loop antenna for LTE/WWAN operations in a smart phone," *Progress In Electromagnetics Research C*, Vol. 16, 147–160, 2010.

16. Chung, Y., et al., "High isolation dual-polarized patch antenna using integrated defected ground structure," *IEEE Microwave and Wireless Components Letters*, Vol. 14, No. 1, 4–6, 2004.

17. Mak, A. C. K., C. R. Rowell, and R. D. Murch, "Isolation enhancement between two closely packed antennas," *IEEE Transactions on Antennas and Propagation*, Vol. 56, No. 11, 3411–3419, 2008.

18. Li, J.-F., et al., "Compact dual band-notched UWB MIMO antenna with high isolation," *IEEE Transactions on Antennas and Propagation*, Vol. 61, No. 9, 4759–4766, 2013.

19. Wong, K.-L., B.-W. Lin, and B. W.-Y. Li, "Dual-band dual inverted-F/loop antennas as a compact decoupled building block for forming eight 3.5/5.8-GHz MIMO antennas in the future smartphone," *Microwave and Optical Technology Letters*, Vol. 59, No. 11, 2715–2721, 2017.

20. Mathur, R. and S. Dwari, "Compact CPW-fed ultrawideband MIMO antenna using hexagonal ring monopole antenna elements," *AEU — International Journal of Electronics and Communications*, 2018.

21. Dabas, T., et al., "Mutual coupling reduction between elements of UWB MIMO antenna using small size uniplanar EBG exhibiting multiple stop bands," *AEU — International Journal of Electronics and Communications*, 2018.

22. Khan, M. S., et al., "A compact CSRR-enabled UWB diversity antenna," *IEEE Antennas and Wireless Propagation Letters*, Vol. 16, 808–812, 2017.

23. Li, Y. and G. Yang, "Dual-mode and triple-band 10-antenna handset array and its multiple-input multiple-output performance evaluation in 5G," *International Journal of RF and Microwave Computer-Aided Engineering*, e21538, 2018.

24. Babu, K. B. V. and B. Anuradha, "Tri-band MIMO antenna for WLAN, WiMAX and defence system & radio astronomy applications," *Advanced Electromagnetics*, Vol. 7, No. 2, 60–67, 2018.

25. Srinivasa Rao, P., K. J. Babu, and A. M. Prasad, "Compact multi-band MIMO antenna with improved isolation," *Progress In Electromagnetics Research M*, Vol. 62, 199–210, 2017.